

# Compact polarization rotators for integrated polarization diversity in InP-based waveguides

Daryl M. Beggs,<sup>1,\*</sup> Michele Midrio,<sup>2</sup> and Thomas F. Krauss<sup>1</sup>

<sup>1</sup>*School of Physics & Astronomy, University of St Andrews, North Haugh, St Andrews, KY16 9SS, UK*

<sup>2</sup>*Dipartimento di Ingegneria Elettrica Gestionale e Meccanica, Universita degli Studi di Udine, viale delle Scienze 208, 33100 Udine, Italy*

\*Corresponding author: daryl.beggs@st-andrews.ac.uk

Received May 11, 2007; revised June 15, 2007; accepted June 18, 2007;  
posted June 21, 2007 (Doc. ID 82985); published July 23, 2007

We present the design, fabrication, and operation of a polarization converter based on angled waveguides in the InP/InGaAsP material system. By combining design elements from mode evolution and birefringent devices, the total device length is kept short (less than  $50\ \mu\text{m}$ ) and the insertion efficiency high at  $81\% \pm 19\%$ , which corresponds to an insertion loss of 1 dB. Devices operate broadband, i.e., the polarization conversion exceeds 15 dB over a 100 nm wavelength range. A polarization rotator with these specifications is a prime candidate for use in an integrated polarization diversity scheme. © 2007 Optical Society of America  
OCIS codes: 130.3120, 230.5440, 230.3990, 220.4000.

Microphotonic devices, such as those based on photonic crystals [1] or microring resonators [2], offer much scope for novel applications, as well as the chance to miniaturize optical components on-chip. Silicon or III–V semiconductors are the most promising materials for realizing microphotonic devices, but as device sizes become smaller, the polarization becomes ever more difficult to control. A general solution to the polarization sensitivity of microphotonic components is a scheme based on polarization diversity [3], which can render devices polarization insensitive, but requires polarization splitters and rotators that can be integrated monolithically with other microphotonic components. Passive polarization rotators have recently been demonstrated and are broadly based on two different design premises—those devices based on mode evolution with asymmetric cross sections [4–8] and those incorporating birefringent sections [9]. The mode evolution devices can provide low-loss operation, as long as coupling to other modes is suppressed; this requires a large device length. On the other hand, devices with birefringent sections can provide ultracompact polarization rotation, but the difficulty of matching the modes at the interfaces to the birefringent section render them unacceptably lossy. To create a design with both the low loss displayed by mode evolution devices and the short lengths displayed by birefringent devices, we have adopted a hybrid approach, which relies on a birefringent section, but where the transition into the birefringent section is tapered to better match the relevant modes.

Our design is based on the fact that the eigenstates of an angled waveguide can have two orthogonal polarization states that are skewed with respect to the waveguide angle and that both of these states can be equally excited by an incoming TE or TM polarized mode; the waveguide width controls the nature of these modes. Very wide ( $>2\ \mu\text{m}$ ) waveguides with angled walls, for example, behave virtually like standard ridge waveguides, a fact that can also be exploited for efficient interfacing to conventional wave-

guide circuitry. Our device consists of a birefringent central section where most of the polarization rotation occurs, with angled input and output tapers, as shown schematically in Fig. 1. Since the tapers and the central section all contribute to the polarization rotation, it is essential to choose the compound length of all three sections correctly, and this was done numerically. The input and output tapers were divided into a number of piecewise constant straight waveguides, whose lengths were set equal to  $1\ \mu\text{m}$ , and whose width was varied in steps of 100 nm. The waveguide was tapered from the widest cross section  $W_{\text{max}}=2.0\ \mu\text{m}$  where, for  $\lambda=1.55\ \mu\text{m}$ , 98% of the power of the fundamental mode is in TE field components, and the remaining 2% is in TM ones. Decreasing TE and increasing TM contents are observed in the fundamental mode with decreasing waveguide width. For instance, when the width of a section  $W_{\text{sect}}=1500\ \text{nm}$ , the TE and TM power contents in the fundamental mode are 90% and 10%, respectively, for  $W_{\text{sect}}=1200\ \text{nm}$ , 69% TE and 31% TM, down to 41% TE and 59% TM for a width of 900 nm.

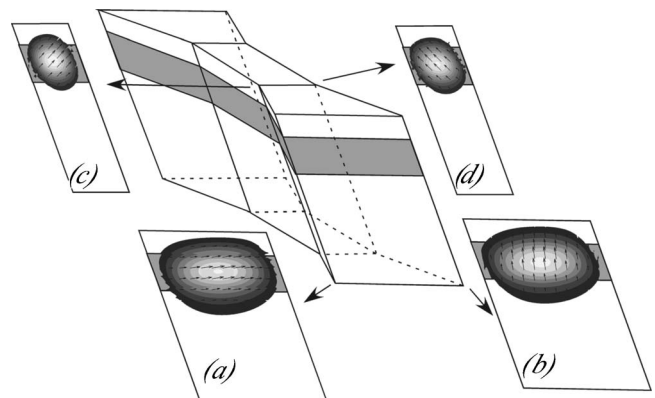


Fig. 1. Schematic of the polarization rotator; the shaded region is the InGaAsP waveguide core. (Inset) the mode profiles and the lines of force for the electric field of the fundamental (a) and second (b) mode of the widest waveguide section; (c) and (d) are the same for the narrowest waveguide section.

All of the above power percentages are reversed in the second mode.

Once the taper was formed, a central waveguide with width  $W=900$  nm and an output taper (identical to the input one) were added. The length of the central waveguide was numerically optimized to obtain the highest polarization conversion, which occurred for a length of  $12.9 \mu\text{m}$  with the conversion efficiency as high as 92.7%. Including the tapers, the overall length of the device is  $L=34.9 \mu\text{m}$ . It should be noted that the choice of  $W$  and  $L$  are not unique. For any given width  $W$ , there will be a length  $L$  that provides the desired polarization rotation, so choosing the value of  $W$  is a trade-off between the final length of the device and the insertion losses.

The InGaAsP heterostructure used in the experiments consists of an InP top cladding (300 nm), an InGaAsP waveguide layer (522 nm), and an InP buffer (1500 nm). A 230 nm thick layer of silica was used as a hard mask, deposited by spin coating commercially available hydrogen silsequioxane [10]. A 200 nm thick layer of poly(methyl methacrylate) (PMMA) was used as a resist, into which the waveguide pattern was defined by electron-beam lithography. Transfer into the hard mask was achieved with reactive ion etching using  $\text{CHF}_3$  chemistry. The deep etching of the InP-based layers was then performed using a high voltage/low current chemically assisted ion beam etching (CAIBE) regime [11] at a high temperature ( $\sim 200^\circ\text{C}$ ), using an angled block to achieve the desired angle of the trenches. An example of the resultant trenches and angled waveguide is shown in Fig. 2. The trenches are etched to a (vertical) depth of over  $6 \mu\text{m}$ , so that the “grass” occurring on the trench floor is sufficiently far from the waveguide core layer to have no effect on its optical properties.

Devices are characterized in an end-fire setup, where light from a tuneable laser is launched via a microscope objective, with the input polarization selected via a beam-splitting polarizer cube. With the laser set to a wavelength of  $\lambda=1.55 \mu\text{m}$ , an analyzer

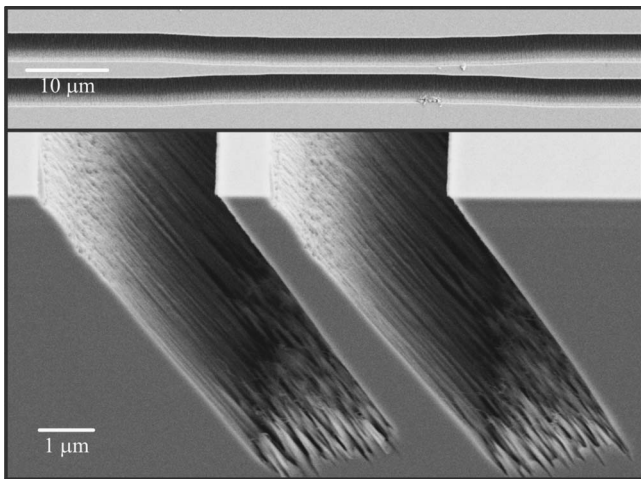


Fig. 2. Scanning electron micrographs of the angled waveguide polarization rotators in InP. Top, a top view, showing the input-output tapers and the central birefringent section. Bottom, a cross section of the deeply etched trenches that define the angled waveguide.

crystal in a rotating mount and an optical compensator were placed on the output side to characterize the output polarization state of the devices. Devices with differing width  $W$  of the central section of the rotator were made, for  $500 \text{ nm} < W < 1500 \text{ nm}$ . Nontapered  $3 \mu\text{m}$  wide waveguides with angled walls were used for comparison. For each value of  $W$ , the output polarization state of the device is determined. Figure 3 shows the rotation of the angle of the plane of polarization (P of P), both for TE (closed squares) and TM (open squares) input as a function of  $W$ . A clear trend can be seen: the rotation is greatest for the narrowest devices and it lessens as the device width is broadened, as expected. Presumably for very broad devices, where  $W \gg \lambda$ , the rotation in the P of P would be zero, but the  $3 \mu\text{m}$  wide straight waveguides are still narrow enough to cause a small rotation of  $(5.0 \pm 2.3)^\circ$ , due to the small hybridity of the modes of an angled waveguide of this width and the long interaction length.

To determine the ellipticity of the output, the phase difference  $\delta$  between the two orthogonal components of the electric field was measured with an optical compensator and is plotted as a function of  $W$  in Fig. 3 (inset). A phase difference of  $\delta=0, \pm\pi$  indicates linearly polarized output, the direction of which is determined by the rotation angle away from the input P of P. For example, the device with a width of 710 nm has a rotation of the P of P of approximately  $180^\circ$ , and the TE (TM) input has a phase difference of  $\delta \approx \pi$  ( $\delta \approx 0$ ). This means that a TE (TM) input gives approximately TE (TM) output, albeit the electric field vector points antiparallel to the input electric field vector. On the other hand, the slightly wider device of width  $W=875$  nm has a rotation of the P of P of very close to  $90^\circ$ , and the TE (TM) input gives a phase difference of  $\delta \approx 0$  ( $\delta \approx \pi$ ) in the output. Thus TE (TM) output has resulted from the orthogonal input.

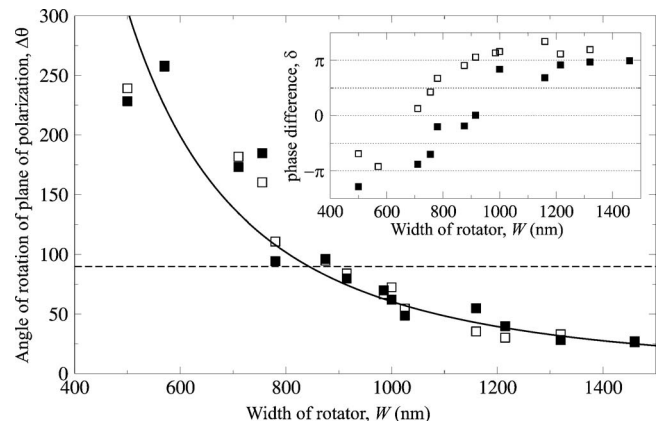


Fig. 3. Measured rotation in the angle of the plane of polarization as a function of the width of the central angled waveguide section for both TE input (closed squares) and TM input (open squares). The solid curve is drawn as a guide to the eye, and the dashed curve indicates the desired rotation angle for polarization conversion operation. (Inset) the measured phase difference between orthogonal components of the electric fields  $\delta$  for the same devices.

The insertion efficiency, determined by taking measurements on 14 different devices with both TE and TM polarizations as input (28 measurements) and comparing the output power with that of 14 measurements on different “blank” waveguides, was found to be  $(81 \pm 19)\%$ , corresponding to an insertion loss of better than 2 dB, with a mean of 1 dB. Obviously, insertion efficiency is a crucial parameter for any device that will be used in integrated photonic circuits, and the insertion efficiency of the devices considered here compares well to other microphotonic polarization rotators; this performance derives from the slowly varying geometry of the designed taper regions while maintaining a very compact footprint. By comparing devices of different lengths, the source of the insertion loss—propagation losses or reflections—can be found, and we estimate that propagation losses are of order  $0.05\text{--}0.1\text{ dB}/\mu\text{m}$  in the central section, meaning that this dominates the total loss: good news, as backreflections can be detrimental to the performance of a photonic circuit.

For a polarization rotator to be used in a general polarization diversity scheme, it must be able to operate over a broad range of wavelengths. Figure 4 shows the polarization conversion ratio of the  $W=875\text{ nm}$  devices. The gray and black bars indicate the wavelength regions for which the conversion ratio exceeds 15 and 20 dB, respectively, for both TE as input (top bars, solid curves) and TM as input (bottom bars, dashed curve). The fringes result from the

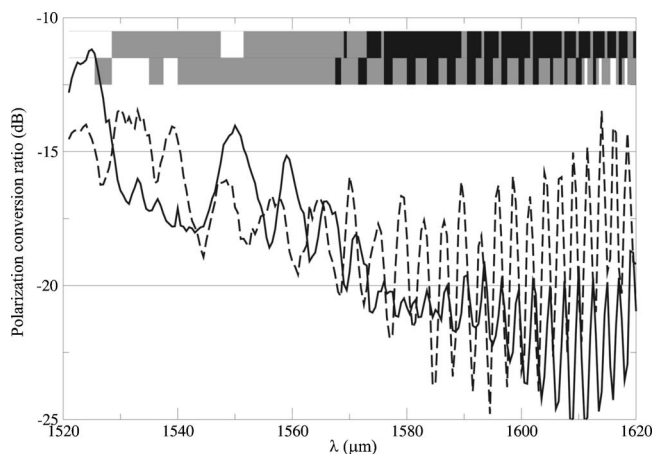


Fig. 4. Polarization conversion ratio [i.e.,  $P(\text{TE})/P(\text{TM})$  for TE input (solid curves) and  $P(\text{TM})/P(\text{TE})$  for TM input (dashed curve)] for the angled waveguide with a central section width of  $W=875\text{ nm}$  as a function of wavelength. The resolution of the measurement was  $0.5\text{ nm}$ . The gray and black bars indicate wavelength ranges for which the conversion ratio exceeds 15 and 20 dB, respectively.

measurement beating against the Fabry–Perot oscillations caused by facet-to-facet reflections on the chip (of length approximately  $2\text{ mm}$ ). These oscillations are therefore unimportant for on-chip integration, and could in any case be eliminated by antireflection coatings at the chip facets. Broadband operation is clearly achieved, with a conversion ratio exceeding 15 dB over almost the entire measured range ( $100\text{ nm}$ ) for both input polarizations. The conversion ratio also exceeds 20 dB for more limited wavelength regions; notably for TE to TM operation, it exceeds 20 dB for a wavelength range of  $\Delta\lambda=50\text{ nm}$ .

In summary, we show that tapered waveguides with angled walls realized in an InP-based material system act as low-loss polarization rotators with a relatively short device length of  $48\text{ }\mu\text{m}$ . The devices match the TE/TM modes of a slab waveguide to the hybrid modes of a narrow birefringent angled waveguide via input and output taper regions. An insertion loss of 1 dB, dominated by propagation rather than reflection losses, and broadband polarization conversion operation (conversion ratio of better than 15 dB over  $100\text{ nm}$  wavelength range for both TE and TM polarizations as input) is demonstrated, which is similar to the performance of other devices reported in the literature but with a shorter device length.

The authors acknowledge the support of the EU-IST “Funfox” STREP project. We also thank Helmut Heidrich of FhG-HHI, Berlin for useful discussions and the loan of an optical compensator.

## References

1. T. F. Krauss, *Phys. World* **19**(2), 32 (2006).
2. F. Xia, L. Sekaric, and Y. Vlasov, *Nat. Photonics* **1**, 65–71 (2007).
3. C. K. Madsen, *Opt. Lett.* **25**, 878 (2000).
4. L. M. Augustin, J. J. G. M. van der Tol, E.-J. Geluk, and M. K. Smit, presented at the European Conference on Integrated Optics, Copenhagen, Denmark, 25–27 April 2007.
5. H. El-Refaei and D. Yevick, *J. Lightwave Technol.* **22**, 1352 (2004).
6. V. P. Tzolov and M. Fontaine, *Opt. Commun.* **127**, 7 (1996).
7. T. Barwicz, M. R. Watts, Milos A. Popovic, P. T. Rakich, L. Socci, F. X. Kartner, E. P. Ippen, and H. I. Smith, *Nat. Photonics* **1**, 57 (2007).
8. M. R. Watts and H. A. Haus, *Opt. Lett.* **30**, 138 (2005).
9. M. V. Kotlyar, L. Bolla, M. Midrio, L. O’Faolain, and T. F. Krauss, *Opt. Express* **13**, 5040 (2005).
10. L. O’Faolain, M. V. Kotlyar, N. Tripathi, R. Wilson, and T. F. Krauss, *J. Vac. Sci. Technol. B* **24**, 336 (2006).
11. M. V. Kotlyar, L. O’Faolain, R. Wilson, and T. F. Krauss, *J. Vac. Sci. Technol. B* **22**, 1788 (2004).